IRAQI JOURNAL OF APPLIED PHYSICS
Vol. 22, No. 4, October-December 2026, pp. 589-595

Walaa R. Nawaaf *
Amjad H. Jassim

Department of Physics,
College of Science,
University of Tikrit,
Tikrit, IRAQ
* Corresponding author email:
Walaa.r.nawaf.phys544@st.tu.edu.iq

Effects of Carbon Nanotubes Concentration on Structural and Optical Characteristics of Bismuth Oxide Films

Thin films of bismuth oxide (Bi_2O_3) reinforced with carbon nanotubes (CNTs) at different concentrations (1-4 wt.%) were prepared on glass substrates and p-type crystalline silicon with (111) orientation. Nonlinear changes in the crystalline structure were revealed with increasing CNT content, reflecting its complex effect on lattice ordering and phase evolution. Morphological studies showed variable changes in surface roughness, with unit variations at the highest concentration, indicating precise modification in particle distribution and surface structure. Changes in emission intensity were revealed, indicating differential improvement in charge separation and reduction of recombination. Optical analysis showed that the UV–Visible spectrum and the corresponding band gap exhibited nonlinear behavior. These results reflect the complex and nonlinear nature of the CNT effect on the structural, morphological, and optical properties of Bi_2O_3 thin films, offering promising opportunities for precise control of these properties for advanced electronic and optoelectronic applications.

Keywords: Thin films; Bismuth oxide (Bi_2O_3); Carbon nanotubes (CNTs); Optical properties

1. Introduction

Metal oxide thin films (MOTFs) are among the most important semiconductor compounds that have attracted wide attention in recent studies due to their distinctive properties, which make them suitable for applications in electronics and optoelectronics, whether as thin or thick layers in various circuits and devices. In this study, thin films of bismuth oxide (Bi_2O_3) doped with different concentrations (1, 2, 3, 4%) of carbon nanotubes (CNTs) were prepared on crystalline silicon (Si-crystal) and glass substrates using the deposition technique, followed by annealing at 200°C. The physical properties of these films - including structural, topographical, and optical characteristics - were investigated, and the effects of doping concentrations and annealing on the internal structure and surface morphology of the films were monitored. Changes in the optical and structural properties of the prepared films were also observed as a result of the different substrate types and CNT concentrations. Crystalline silicon and glass substrates were selected to compare the effect of surface nature on the physical properties.

2. Experimental Part

Thin films of Bi_2O_3 reinforced with CNTs at different concentrations (1, 2, 3, 4%) were prepared by adding the respective CNT mass to 1 g of Bi_2O_3. Glass and p-type crystalline silicon substrates with (111) orientation and resistivity ranging in 1.5-4 Ω.cm were used. The materials were ground and weighed, and the powders were thoroughly mixed for 30 min to ensure homogeneity of the components, then the samples were pressed for 5 min under a pressure of 5 tons. Deposition was carried out using the pulsed deposition technique with 140 pulses, where the energy of each pulse was 400 mJ, while the initial chamber pressure was reduced to 10^{-3} Torr and the distance between the target and the substrate was 2 cm. Subsequently, thermal annealing of the samples was performed at 200°C for 30 min to study the effect of doping on the crystalline structure, surface morphology, and optical properties.

3. Results and Discussion

The XRD patterns of Bi_2O_3 thin films deposited on glass substrates revealed that the main crystalline phase was retained with noticeable variations in peak positions (2θ), inter-planar spacing (d-spacing), and crystallite size. As shown in Fig. (1), for 1% CNTs, peaks appeared at 27.95°, 31.65°, 32.73°, 46.19°, 46.97°, 54.25°, 55.53°, 57.76°, corresponding to the (222), (004), (400), (404), (440), (226), (622), and (444) planes, respectively, according to ICDD card no. 00-022-0515, with crystallite sizes ranging from 23.30 to 30.98 nm. These results indicate that low CNTs doping improved crystallinity and lattice regularity while maintaining the main phase, and no peaks corresponding to CNTs were observed at this low concentration, consistent with other studies [1,2]. For 2% CNTs, peaks were recorded at 27.94°, 31.69°, 32.71°, 46.21°, 46.91°, 54.16°, 55.53°, and 57.75°, corresponding to the (201), (002), (220), (222), (400), (203), (421), and (402) planes, respectively, with a slight increase in crystallite size compared to 1%, ranging from 27.96 to 38.73 nm (ICDD card no. 01-078-1793). A clear CNT peak appeared at 27.06°, corresponding to the (002) plane.

At 3% CNTs, peaks appeared at 27.24°, 31.81°, 32.80°, 46.28°, 47.08°, 54.20°, 55.64°, and 57.79°, corresponding to the (222), (004), (400), (404), (440), (226), (622), and (444) planes, respectively, while the

crystallite size sharply decreased to 1.59-3.27 nm, consistent with ICDD card no. 00-022-0515. This reduction is attributed to increased defects and lattice strain due to CNTs accumulation at grain boundaries, hindering crystal growth. The CNTs peak at 27.06° (002) was observed. For 4% CNTs, the XRD pattern matched ICDD card no. 00-022-0515, with main peaks at 27.93°, 31.68°, 32.69°, 46.20°, 46.94°, 54.24°, 55.53°, and 57.76°, corresponding to (222), (004), (400), (404), (440), (226), (622), and (444), respectively. Compared to 3%, the crystalline pattern partially recovered, and the crystallite size increased to 23.30-38.73 nm, indicating a structural balance where CNTs integrate into the lattice or grain boundaries without forming a separate secondary phase. Crystallite size (D_{avg}) was calculated using Scherrer's equation: $D_{avg} = \frac{0.89\lambda}{\beta \cos\theta}$ [3], confirming that the crystallite size of CNTs-doped Bi_2O_3 thin films does not increase linearly with doping concentration but passes through distinct stages [4].

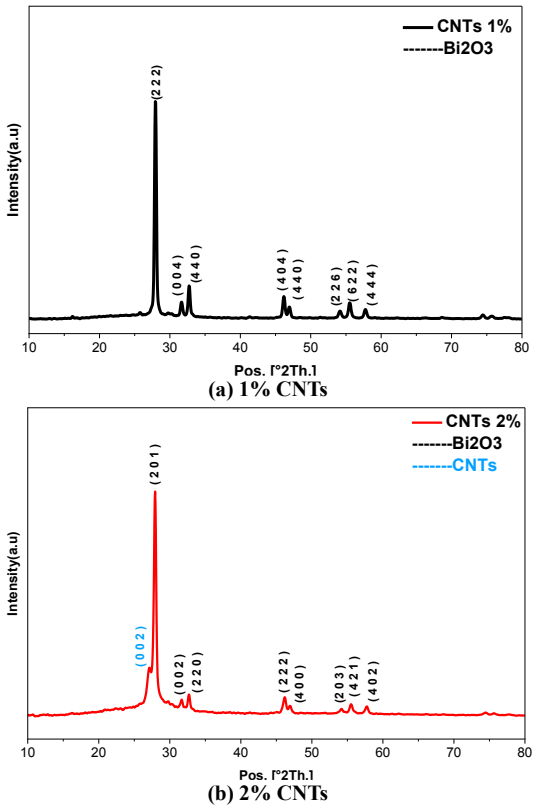

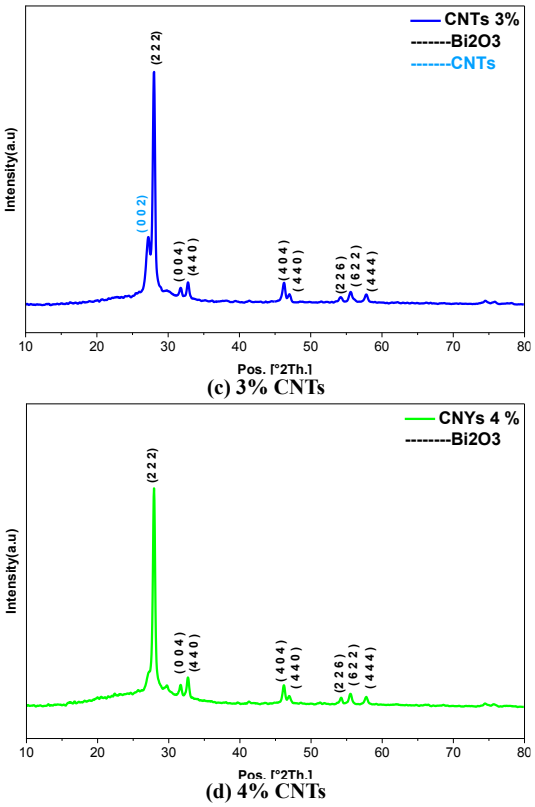

Fig. (1) XRD patterns of Bi_2O_3 thin films deposited on glass and doped with (a) 1% CNTs, (b) 2% CNTs, (c) 3% CNTs, and (d) 4% CNTs

On silicon substrates, XRD patterns revealed similar main peaks. As shown in Fig. (2), at 1% CNTs, main peaks appeared at 27.97°, 32.71°, 46.22°, 46.95°, 55.48°, and 57.84°, corresponding to (222), (400), (404), (440), (622), and (444), respectively, with crystallite sizes ranging from 9.55 to 38.73 nm (ICDD card no. 00-022-0515), indicating relatively good crystal growth. At 2% CNTs, diffraction patterns matched ICDD card no. 00-022-0515, with peaks at 27.97°, 32.72°, 46.25°, 46.99°, 55.55°, and 57.84°, and crystallite sizes increased to 19.10-38.73 nm. At 3% CNTs, peaks were observed at 28.45°, 32.72°, 46.97°, and 55.53°, corresponding to (111), (200), (220), and (311) planes, respectively (ICDD card no. 00-032-0956), with very small crystallite sizes of 1.65-3.13 nm. This sharp decrease reflects the significant role of high CNTs content in increasing nucleation sites and inhibiting crystal growth, along with introducing lattice strain. At 4% CNTs, peaks at 28.47°, 32.73°, 46.96°, 55.53°, and 58.80° corresponding to (111), (200), (220), (311), and (222), respectively, were observed, with crystallite sizes ranging from 28.51 to 51.59 nm (ICDD card no. 00-022-0515), indicating recrystallization compared to 3%, partial CNTs redistribution at grain boundaries, and improved crystal growth.

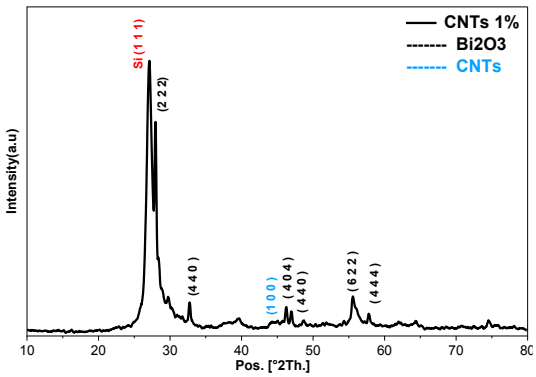

(a) 1% CNTs

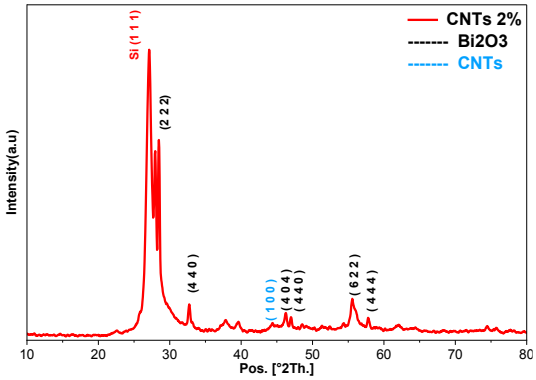

(b) 2% CNTs

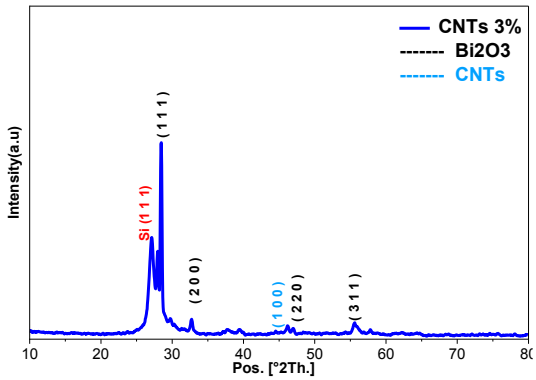

(c) 3% CNTs

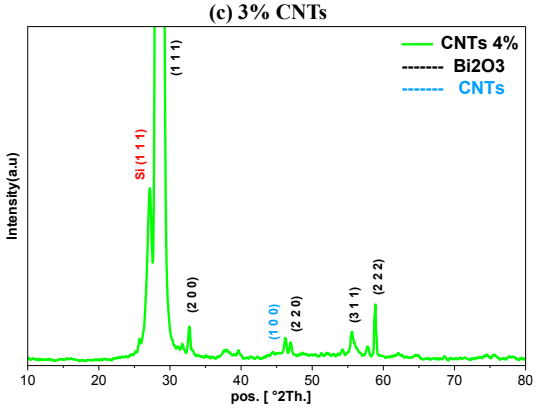

(d) 4% CNTs

Fig. (2) XRD patterns of Bi_2O_3 thin films deposited on silicon and doped with (a) 1% CNTs, (b) 2% CNTs, (c) 3% CNTs, and (d) 4% CNTs

A CNTs signal at 44° (100) appeared in all samples due to reduced substrate influence. The results highlight notable differences between substrates: CNTs peaks at 44° (100) appeared on silicon due to surface roughness promoting certain crystalline orientations, whereas these peaks were weak or absent on smooth glass surfaces, where film adherence and peak intensity were reduced within the 42°-44° angular range.

Atomic force microscopy (AFM) was performed to investigate the effect of carbon nanotubes (CNTs) doping on the surface morphology of Bi_2O_3 films deposited on glass and (111)-oriented crystalline silicon substrates. The results revealed a nonlinear variation in surface roughness (RMS) and average deviations (Sa) with increasing CNTs concentration, due to the interplay between nucleation and growth mechanisms, lattice matching, aggregation of the dopants, and internal strain. On glass substrates, at 1% CNTs, relatively high roughness was observed (RMS = 3.88 nm, Sa = 2.79 nm), reflecting the presence of localized aggregates and surface irregularities. At 2% CNTs, roughness decreased (RMS = 1.73 nm, Sa = 1.39 nm), indicating a homogeneous distribution of CNTs and surface improvement. At 3%, roughness increased again (RMS = 3.35 nm, Sa = 2.31 nm) due to the formation of new aggregates, with smaller and more uniform grains. At 4%, the highest roughness was recorded (RMS = 4.28 nm, Sa = 2.78 nm), indicating saturation of doping and the emergence of large clusters at higher CNTs concentrations [1]. Increased roughness is a critical factor in solar cell applications as it enhances electromagnetic radiation absorption and improves cell efficiency [5]. These observations suggest that the optimal CNTs doping for balancing structural homogeneity and surface roughness is 2%, as illustrated in Fig. (3) and table (1).

Table (1) Variation of surface roughness and average deviations with changing doping concentration on glass substrates

Doping ratio	RMS Roughness (Sq) (nm)	Main roughness (Sa) (nm)
1%	3.88312	2.79627
2%	1.73408	1.39519
3%	3.35417	2.31215
4%	4.28962	2.78071

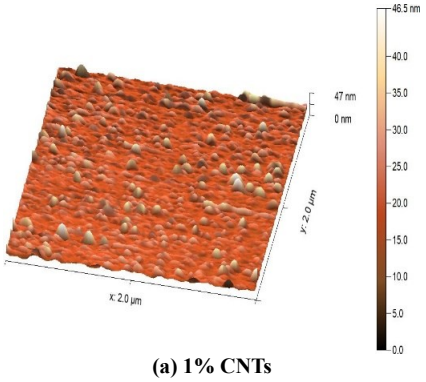

(a) 1% CNTs

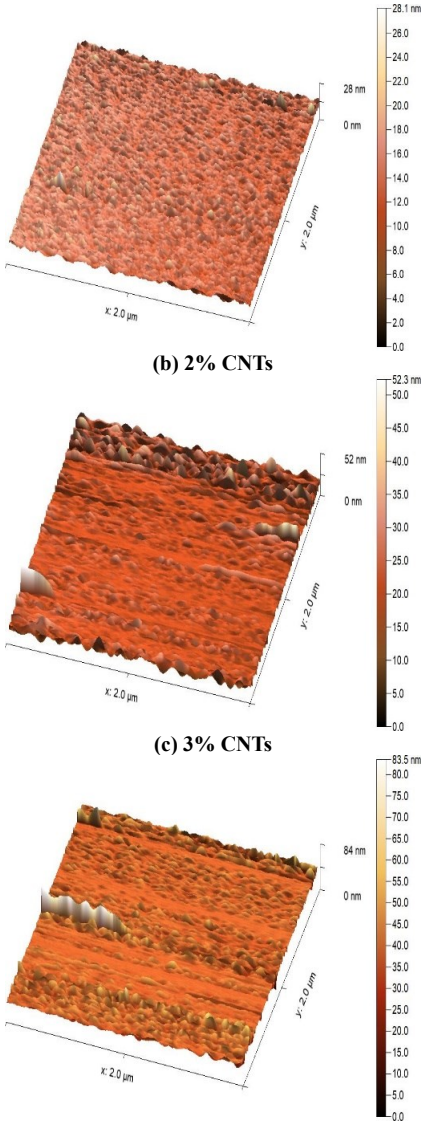

Fig. (3) 3D AFM images of Bi_2O_3 thin films deposited on glass, doped with (a) 1% CNTs, (b) 2% CNTs, (c) 3% CNTs, and (d) 4% CNTs, and annealed at 200°C for 30min

On (111) crystalline silicon substrates, at 1% CNTs, moderate roughness (12.8 nm) was observed, increasing to 16.9 nm at 2% due to local cluster formation and increased topographical contrast. At 3%, roughness decreased slightly to 15.6 nm as a result of improved structural distribution and gap filling, while at 4%, a sharp decrease to 0.68 nm was noted, reflecting surface reorganization and reduction of clustering [6]. Overall, the contrast in roughness between glass and silicon substrates highlights the influence of substrate properties, where surface crystallinity, amorphicity, and roughness affect CNTs distribution and grain size, consistent with previous studies on substrate effects on film structure [7]. Figure (4) and table (2) summarize these observations.

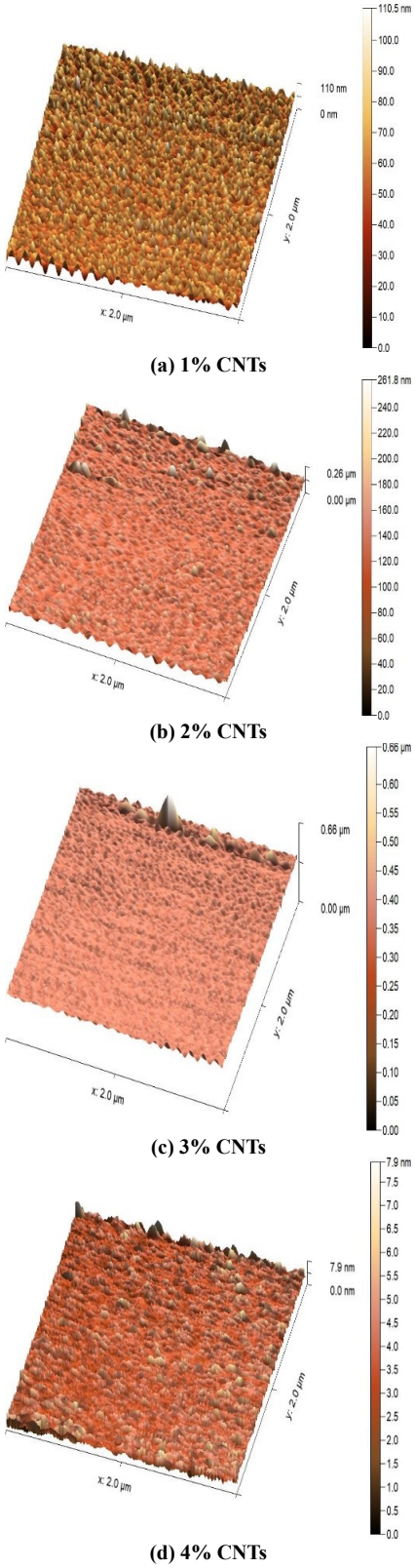

Fig. (4) 3D AFM images of Bi_2O_3 thin films deposited on silicon, doped with (a) 1% CNTs, (b) 2% CNTs, (c) 3% CNTs, and (d) 4% CNTs, and annealed at 200°C for 30min

Table (2) Variation of surface roughness and average deviations with changing doping concentration on silicon substrates

Doping ratio	RMS Roughness (Sq) (nm)	Main roughness (Sa) (nm)
1%	12.8196	10.1883
2%	16.9780	12.8127
3%	15.6169	10.9899
4%	0.860217	0.676859

The optical properties of the films deposited on silicon were also investigated using photoluminescence (PL) spectroscopy to evaluate the band gap, crystal quality, and the presence of defects. The results showed a clear variation in the band gap with increasing CNTs content. At 1% and 2% CNTs, the samples exhibited lower band gaps of 1.862 eV at 664.367 nm and 1.902 eV at 652.454 nm in the red light region, reflecting the influence of defects and oxygen vacancies on the crystal structure. At 3% CNTs, the band gap increased significantly to 2.995 eV at 413.995 nm in the violet–blue region, which can be attributed to the phase transition to γ-Bi_2O_3, quantum confinement effects due to reduced crystallite size, and the possible Burstein–Moss shift resulting from increased carrier concentration. At 4% CNTs, the band gap decreased to 1.8878 eV at 661.137 nm (table 3) due to CNTs aggregation and the generation of additional defects, which limit electronic transport efficiency and introduce states within the gap that provide non-radiative recombination pathways, reducing emission intensity.

These results indicate that the effect of CNTs on the optical properties strongly depends on the doping concentration: low concentrations (1–2%) lead to limited improvement, medium concentration 3% significantly widens the band gap, while higher concentrations 4% deteriorate the properties due to defects and aggregation. These findings are consistent with previous studies on the effect of dark exciton states in multi-walled carbon nanotubes (MECNTs) [8]. Figure (5) shows the PL spectra of the samples on crystalline silicon.

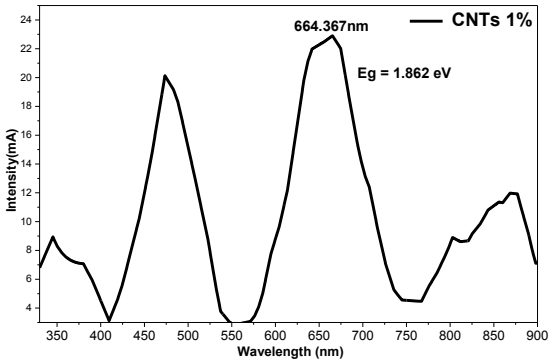

(a) 1% CNTs

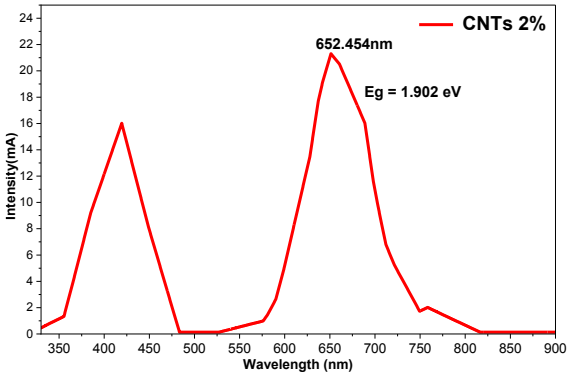

(b) 2% CNTs

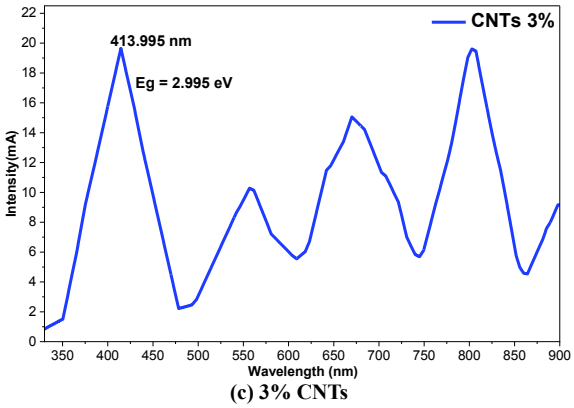

(c) 3% CNTs

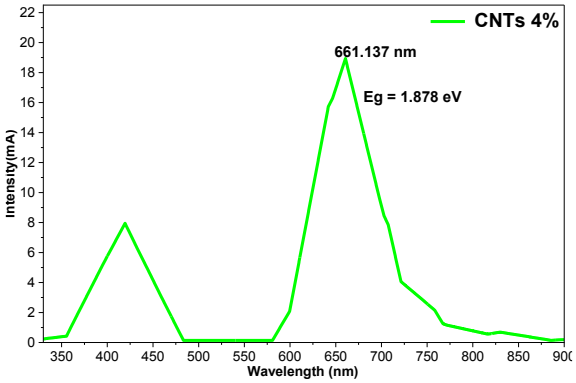

(d) 4% CNTs

Fig. (5) PL spectra of Bi_2O_3 thin films doped with (a) 1% CNTs, (b) 2% CNTs, (c) 3% CNTs, and (d) 4% CNTs

Table (3) PL results of Bi_2O_3 thin films doped with carbon nanotubes and deposited on silicon substrates

Sample	Wavelength (nm)	E_g (eV)
1% CNTs	664.367	1.862
2% CNTs	652.454	1.902
3% CNTs	413.995	2.995
4% CNTs	661.137	1.878

The UV-visible absorption spectra exhibited strong absorption at short wavelengths (300-450 nm) due to direct electronic transitions, while absorption decreased at longer wavelengths (450-1100 nm). The addition of 1% CNTs significantly enhanced absorption by broadening the spectral range and improving surface properties, whereas increasing the concentration to 2% and 3% led to a relative decrease due to CNTs

aggregation and loss of homogeneity. At 4% CNTs, absorption increased again in the short-wavelength region while remaining low at longer wavelengths. Thermal annealing improved the crystalline structure, reduced structural defects, and enhanced optical properties, rendering the films suitable for optoelectronic and photovoltaic applications such as solar cells and photodetectors (Fig. 6).

The direct allowed band gap (E_g) was calculated using the relation $\alpha h\nu = B\left(h\nu - E_g\right)^r$ [9] and applying the Tauc method to the absorption spectra, where the plot of $(\alpha h\nu)^2$ versus photon energy ($h\nu$) is extrapolated to the absorption edge to determine E_g [10]. The results, summarized in table (4), showed band gaps of 2.673 eV at 1% CNTs, 1.581 eV at 2%, 3.270 eV at 3%, and 3.158 eV at 4%, within the semiconductor range of 2.0-3.9 eV. The sharp decrease at 2% is attributed to mid-gap states, oxygen vacancies, or amorphous regions (Urbach tails), reflecting CNTs-induced band gap narrowing [10,11]. The increase at 3% and slight decrease at 4% indicate nonlinear behavior due to the Burstein–Moss effect, possible phase transitions or crystallite size changes, and CNTs aggregation affecting charge distribution. Thus, the nonlinear band gap behavior at 3-4% CNTs results from overlapping structural and electronic effects, consistent with previous studies [12]. The results indicate that CNTs incorporation significantly influences energy levels and reduces some structural defects, enhancing band gap stability and optical response, making these films suitable for optoelectronic applications. Figure (7) shows the band gaps of all samples.

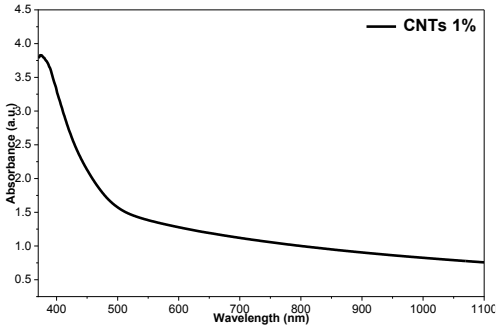

(a) 1% CNTs

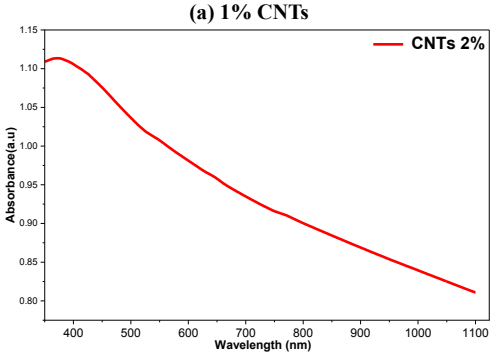

(b) 2% CNTs

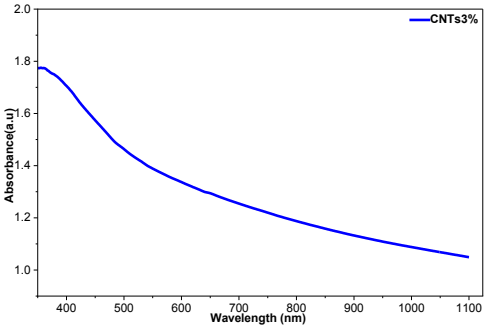

(c) 3% CNTs

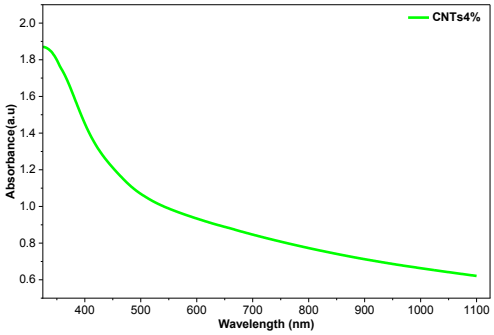

(d) 4% CNTs

Fig. (6) UV-visible absorption spectra of Bi_2O_3 thin films doped with (a) 1% CNTs, (b) 2% CNTs, (c) 3% CNTs, and (d) 4% CNTs

Table (4) Band gap values at different CNTs doping concentrations

Sample	E_g (eV)
1% CNTs	2.673
2% CNTs	1.581
3% CNTs	3.270
4% CNTs	3.158

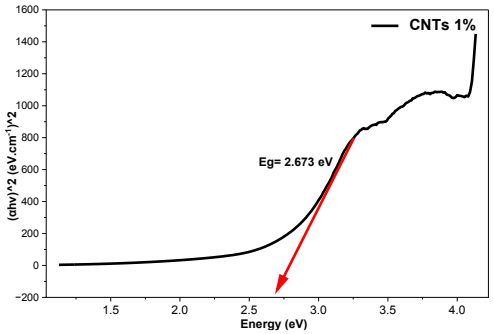

(a) 1% CNTs

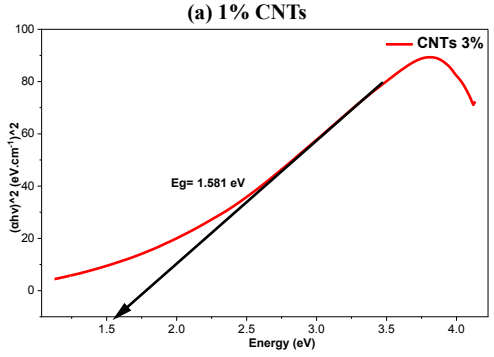

(b) 2% CNTs

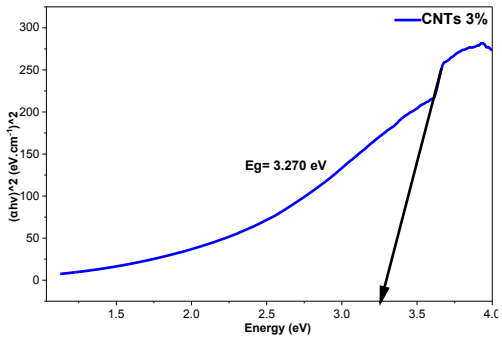

(c) 3% CNTs

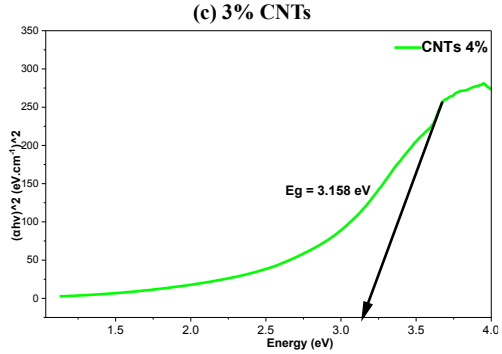

(d) 4% CNTs

Fig. (7) Determination of energy ban gap of Bi_2O_3 thin films doped with (a) 1% CNTs, (b) 2% CNTs, (c) 3% CNTs, and (d) 4% CNTs

References

[1] T.Y. Sabri and A.S. Jasim, "Effect of MWCNT Concentration on Characteristics of Bi_2O_3/MWCNT Nanocomposite Films Prepared by Pulsed-Laser Deposition", 21(1) (2025) 139-144.

[2] R. Vyas et al., "Synthesis and Hydrogen Sensing Properties of CNT-ZnO Nanocomposite Thin Films", *Int. J. Mod. Phys. Conf. Ser.*, 22 (2013) 478-482.

[3] A. Bishnoi, S. Kumar and N. Joshi, "Wide-angle X-ray diffraction (WXRD): technique for characterization of nanomaterials and polymer nanocomposites", in **Microscopy Methods in Nanomaterials Characterization**, Elsevier (2017), pp. 313-337.

[4] B.A. Hasan et al., "Structural, morphology and optical properties of AlxSb1-x thin films prepared by Pulsed laser deposition (PLD)", *AIP Conf. Proceed.*, 2372 (2021) 040010.

[5] R.A. Ahmed et al., "Synthesis and Characterization of $CdO_{1-x}ZnO_x$ for Solar Cell Applications", *Digest J. Nanomater. Biostruct.,* 14(1) (2019) 15-22.

[6] A.S. Maktoof, G.H. Mohammed and H.H. Abbas, "Effect of annealing process on structural and optical properties of Au-doped thin films (NiO:WO_3) fabricated by PLD technique", *J. Opt. (India)*, 54 (2024) 2204-2215.

[7] M. Kellegöz and S. Kurtaran, "Optical and Morphology Mechanism of CeO_2 Thin Films Prepared by Ultrasonic Spray Pyrolysis Method", *Sakarya Univ. J. Sci.,* 28(6) (2024) 1285-1295.

[8] K.F. Chan et al., "Tuning the optical bandgap of multi-walled carbon nanotube-modified zinc silicate glass-ceramic composites", *Ceram. Int.*, 47(14) (2021) 20108-20116.

[9] A.V. Rzhanov and K.K. Svitashev, "Ellipsometric Techniques to Study Surfaces and Thin Films", *Adv. Electron. Electron Phys.*, 49 (1979) 1-84.

[10] P.M.A.K. Sone et al., "Innovative ternary bismuth oxychloride/bismuth oxide/carbon nanotubes induced excellent solar light-driven activity toward photomineralisation of diclofenac: Impact of metastable β-Bi_2O_3 inserted and electron-hole separation", *Result. Chem.*, 7 (2024) 101497.

[11] J. Cai et al., "Effect of calcination temperature on structural properties and photocatalytic activity of Mn-C-codoped TiO_2", *Mater. Res.*, 19(2) (2016) 401-407.

[12] A. Bielicka–Giełdoń et al., "Effect of multi-walled carbon nanotubes properties on the photocatalytic activity of bismuth-based composites synthesised via an imidazolium ionic liquid", *Appl. Surf. Sci.*, 663 (2024) 160214.

